Multinucleon-transfer reactions for the $^{50}Ti+^{93}Nb$ system at sub- and near-barrier energies

H. J. Kim, J. Gomez del Campo, D. Shapira, and P. H. Stelson
Oak Ridge National Laboratory, Oak Ridge, Tennessee 37831

D. Napoli
Legnaro National Laboratory, Legnaro, Italy
(Received 14 August 1990)

Target and target-like ejectiles emitted forward from ^{93}Nb-beam bombardment of thin ^{50}Ti targets were investigated at sub- and near-barrier energies using a magnetic spectrograph. Reaction products from three single-nucleon-transfer and seven multinucleon-transfer channels were observed. Multinucleon-transfer products were observed with a sharp onset only for those collisions with apsidal distances smaller than about 12.6 fm, while single-nucleon-transfer products were observed throughout the apsidal distance range studied. Average Q values of the multinucleon-transfer-reaction products are much more negative than the respective optimum values. These results suggest the formation of a neck at subbarrier energies.

I. INTRODUCTION

A number of diverse theories can account, to a similar extent, for experimentally observed large enhancements in sub-barrier fusion cross sections. For example, coupled-channels,[1] neck-formation,[2] distributed-barrier,[3] and direct absorption[4] theories have been used, with comparable degrees of success, to analyze the enhancement in $^{58}Ni+^{58}Ni$ fusion cross sections at sub-barrier energies. This example illustrates that, although necessary, fusion cross sections alone are not sufficient to assess what really is the underlying enhancement mechanism.

Although their details vary, these theories share a reliance on interactions between the incident and one or more outgoing reaction channels to produce the enhancement. Being microscopic, the coupled-channels approach requires interactions with specific individual exit channels, such as inelastic and nucleon-transfer. On the other hand, being macroscopic in nature, the neck-formation and distributed-barrier theories treat the interactions in a more global way. Thus, in addition to fusion, detailed studies of exit channels in general at sub-barrier energies are very much needed in order to develop a good theoretical understanding of how the enhancement really comes about. However, only limited experimental data of this kind exist.

A rare example of such studies is Wolf's report[5] of deep-inelastic reactions between ^{58}Ni and $^{112,124}Sn$ at sub-barrier energies. Wolf reported significant yields of products from deep-inelastic reactions at subbarrier energies, thus demonstrating the presence of many exit channels that share the incident flux with fusion, even at subbarrier energies. However, because of the inclusive nature of the results of this pioneering experiment, information about the identity and strength of individual channels populated is not available. Stefanini *et al.*[6] investigated transfer reactions for the $^{32,36}S+^{58,64}Ni$ systems at near-barrier energies. There they found differential cross sections to have bell-shaped distributions around the grazing angle, which are characteristic of peripheral collisions. Theoretical fusion cross sections calculated in coupled-channels formalism using transfer strengths determined from these near-barrier data generally are satisfactory, even down at sub-barrier energies. However, the validity of calculated results become questionable at sub-barrier energies because the transfer strengths may change with energy. More recently, Corradi *et al.*[7] investigated transfer reactions and their effect on the fusion for the $^{33}S+^{90,91,92}Zr$ systems, but at energies where fusion cross sections are large (about 100 mb and larger), not at sub-barrier energies.

We report here the measurement of intensities and energies of element (Z) and mass (M) identified fragments from binary exit channels from the $^{50}Ti+^{93}Nb$ reaction in the energy region where the fusion cross section changes from less than 1 to about 40 mb. Figure 1 shows

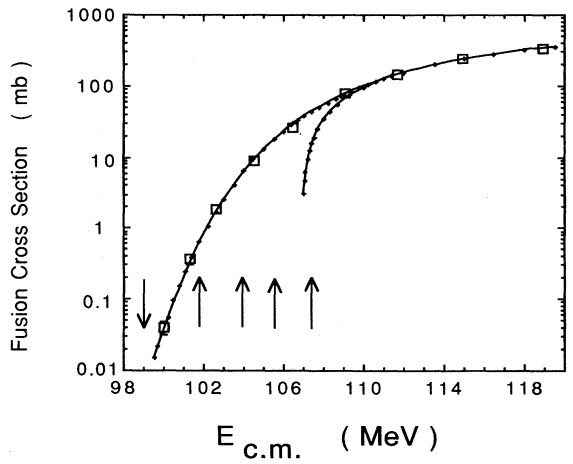

FIG. 1. Fusion cross sections for the $^{50}Ti+^{93}Nb$ system. Squares and crosses are experimental and calculated results, respectively. Solid curves join the calculated results for single and distributed barrier cases. See Ref. 8 for detail. The arrows indicate where the measurements reported in this paper were made.

the fusion cross sections[8] covering this energy range. Our primary objective was to determine the identity and strengths of reaction channels that share the incident flux with, or compete against, the fusion channel at these sub-barrier energies.

Observations of multinucleon-transfer products at low energies have already been reported.[9] But, the earlier results were based on either radiochemical or radioactivity measurements and the data are correspondingly limited. Present results are more comprehensive and thus very amenable to a closer scrutiny.

II. EXPERIMENT DETAIL AND RESULTS

A. General

The experimental arrangement is the same as that of our previous study of the ^{50}Ti+^{90}Zr reaction.[10] Briefly, target and targetlike ejectiles emitted forward from the bombardment of thin (about 30 μg/cm^2) ^{50}Ti targets by ^{93}Nb beams were first magnetically analyzed and then detected by a hybrid position-sensitive gas detector, which was placed near the nominal focal plane of the magnet. Isotopic content of the target is 98.2% ^{50}Ti, 1.5% ^{48}Ti, and a trace amount ($<0.2\%$) of ^{47}Ti and ^{46}Ti. Ejectiles emitted in $10^\circ<\theta<20^\circ$ angular range were investigated at bombarding energies of 283.1, 291.2, 297.2, 302.0, and 306.9 MeV. The corresponding c.m. angular range and energies are 140°–160° (for elastics) and 99.0, 101.8, 103.9, 105.6, and 107.3 MeV. A Si(Au) detector, placed at 32° relative to the beam direction, monitored scattered beam and target recoil intensities. The monitor count and the integrated beam current were used to obtain absolute values of cross sections.

B. Identification of ejectiles

Using the heavier collision partner as projectiles resulted in energetic (<220 MeV) ejectiles, which resulted in good ΔE and E resolutions. Typical Z spectra, obtained from $\Delta E-E$ plots by projecting onto an axis determined by using a simple expression $\Delta E \propto E$, are shown in Fig. 2. Subsequent to Z selection, the M selection was effected from either E vs ρB or E vs $\rho B/\sqrt{E}$ plot. Here E is the ejectile energy and B is the magnetic rigidity (note that $\rho B/\sqrt{E}$ is proportional to $\sqrt{M}/q$, where q is the ionic charge). Representative $\sqrt{M}/q$ spectra are shown in Fig. 3. Both the Z and $\sqrt{M}/q$ resolutions were good enough for unambiguous identification of all significant peaks. The ^{48}Ti peaks seen in the 101.8-MeV spectrum [Fig. 3(a)] are due to about 1.5% isotopic contaminants present in the target. The strength of ^{48}Ti peak seen in Fig. 3(b) exceeds 1.5%, indicating a contribution from the ^{50}Ti$\rightarrow^{48}$Ti two-neutron transfer reaction to the peak at the higher energy. The presence of this contaminant peak materially aided the calibration of $\sqrt{M}/q$ dispersion. Elastic scattering results from a thin ^{51}V target at the lowest bombarding energy were also helpful for the Z and $\sqrt{M}/q$ calibrations.

Nuclides that are definitely from the ^{50}Ti+^{93}Nb reactions are titanium ($Z=22$) isotopes $M=48,49,50,51,52$; vanadium ($Z=23$) isotopes $M=51,52,53$; chromium

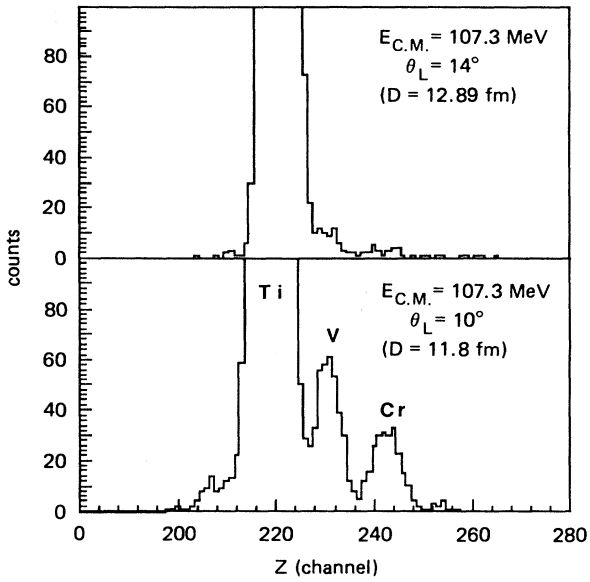

FIG. 2. Typical Z spectra at two energies obtained from $\Delta E-E$ plots assuming $\Delta E \propto E$.

($Z=34$) isotopes $M=52,53,54$. It is noteworthy that, whereas the titanium isotopes are distributed around the initial mass $M=50$, the vanadium and chromium isotopes are heavier than $M=50$ and 51, respectively. This shows that whenever a situation calls for both proton and neutron transfer, the neutron's direction of transfer is the same as that of the proton: i.e., the proton and neutron never go opposite ways. Of these 11 nuclides, only ^{49,50,51}Ti and ^{51}V, all of which result from single neutron- or proton-transfer reaction, were observed at $E<103.9$ MeV.

C. Energy spectra

Energy spectra of reaction products were obtained from E vs $\sqrt{M}/q$ plots by projecting two central $\sqrt{M}/q$ peaks onto the E axis and summing the results channel by channel. Spectra obtained in this manner for two representative energies are shown in Figs. 4 and 5. The energy scale was established by equating the pulse height of the ^{50}Ti peak at the lowest bombarding energy, where the peak is the sharpest, to the energy calculated assuming elastic collision. For reference, the locations of the ground-state–ground-state transition (Q_{gg}) are indicated by the vertical lines. We note the following characteristics from these and other energy spectra: (a) Single skewed peak with low-energy shoulder but centered or nearly centered around Q_{gg} dominates the incident and all single-nucleon-transfer channel spectra; this peak is narrower and more symmetric at the lowest bombarding energy [see Figs. 4 and 5(a)]. (b) A broad bump, located away from Q_{gg} by as much as -10 MeV, characterizes energy spectra of all exit channels that require transfer of one or more protons, plus one or more neutrons, hereafter termed multinucleon-transfer channels, [see Figs. 5(b) and 5(c)]. (c) The difference between the average and the

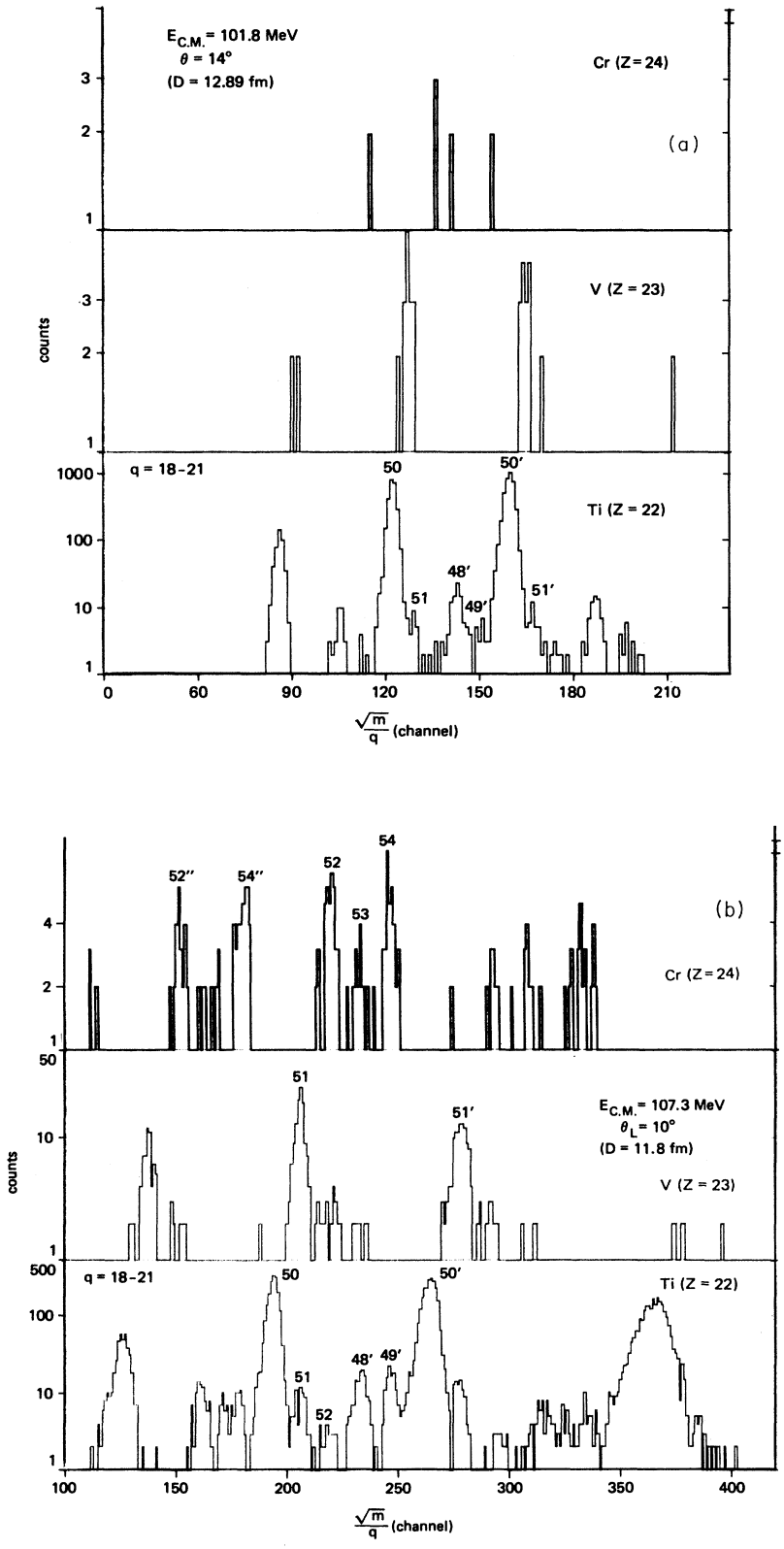

FIG. 3. (a) Z gated $\sqrt{M}/q$ spectra just below the onset of multinucleon-transfer reactions. Numbers accompanying the peaks are M: unprimed numbers for the most probable charge state q and primed for other q. $M=48$ peak is due to about 1.5% ^{48}Ti target contaminant. (b) Z gated $\sqrt{M}/q$ spectra above the onset. See the caption for Fig. 3(a) for the numbers accompanying the peaks.

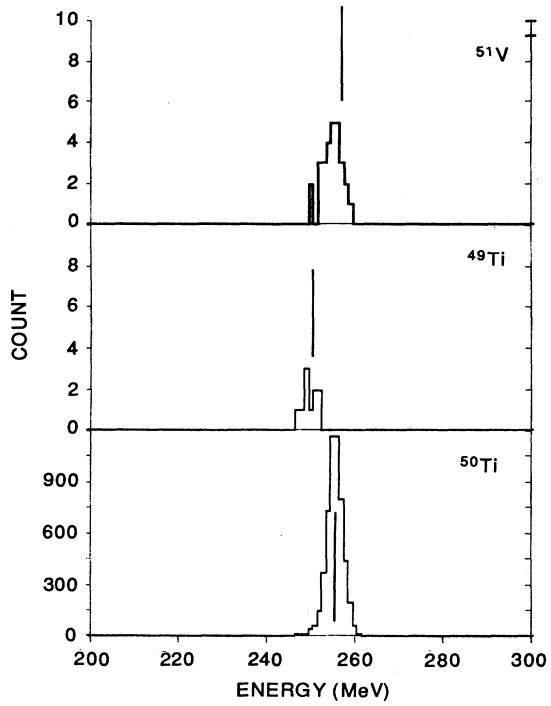

FIG. 4. Energy spectra of the reaction products shown in Fig. 3(a). The heavy vertical lines show the positions of Q_{gg}.

g.s.-g.s. Q value generally increases with increasing number of nucleons transferred [see Figs. 5(b) and 5(c) and Table I).

It is possible that some of the nuclei originally produced by multinucleon-transfer reactions are so highly excited that they may evaporate nucleons and become lighter, e.g., $^{54}Cr \rightarrow {}^{53}Cr + n$ or $^{53}V + p$. However, there is no evidence for the presence of evaporation bumps [e.g., Figs. 5(b) and 5(c)]. Accordingly, all eleven nuclides enumerated above are primary reaction products from such binary reactions as Ti(^{93}Nb, ^{54}Cr)^{89}Y, ^{50}Ti(^{93}Nb,^{53}V)^{90}Zr, etc.

D. Reaction product yield

The strength of the magnetic spectrograph was set to position the strongest $\sqrt{M}/q$ peak or peaks of the incident channel in the center of the detector for all runs. With this procedure, four charge states were covered simultaneously for all relevant channels for most runs. Observed q dependence of intensities agrees well with that of Sayer,[11] and the summed intensity of these charge states exceeds 90% of the total for the Ti ($Z=22$), V ($Z=23$), and Cr ($Z=24$) isotopes. However, in order to free the results from variations in detection efficiency that can arise due to "edge" effects, we used only the counts from two central peaks in the reaction strength or yield consideration. Yields determined in this manner can be converted to absolute cross sections after correcting for the charge-state dependence. This step is shown below.

E. Angular distributions

Angular distributions of quasielectric cross sections are shown in Fig. 6. As shown in Ref. 10, quasielastic cross sections σ_{qe}, which are the sum of cross sections from all observed exit channels, including the incident channel, are convenient quantities for defining transfer probabilities, since they represent the totality of incident flux shared amongst the reaction channels, excluding the absorbed portion. (In addition, the resolution was not adequate to isolate elastics cleanly.) The incident channel contribution to the quasielastic cross sections is 90% or more at all energies except the highest. Thus, even though we used elastic-scattering relations to transform quasielastic cross sections and angles from the laboratory to the center-of-mass system, the results are accurate enough for the purposes at hand. Besides, transformation factors (e.g., the Jacobian) are nearly the same for all channels, owing to the quasielastic nature of the reactions and to the adoption of the reversed-kinematics technique. Only ^{50}Ti ejectiles were observed at the lowest (99.0 MeV) energy; the yield of ^{50}Ti at this energy and at $\theta=140°$ was assumed to result from pure Rutherford scattering (i.e., $d\sigma_{qe}/d\sigma_R = 1$).

The value of $d\sigma_{qe}/d\sigma_R$ is close to one in the angular range studied for the three lower energies. This indicates little absorption of incident flux into fusion and other unobserved channels. The cross section ratio, however, begins to drop markedly with angle starting at about 148° at the highest energy, indicating the onset of severe absorption at this particular angle and energy. The maximum absorption is 43%, which is still much less than the quarter-point absorption (75%).

Angular distributions of reaction products for two representative exit channels are shown in Figs. 7 and 8. Results for other exit channels are similarly devoid of structures. Average Q values, given in Table I, were used for laboratory-to-c.m. transformations. Absolute cross-

TABLE I. Q values for $E_{c.m.} = 107.3$ MeV and $\theta_l = 14°$ results.

Reaction	(^{50}Ti,^{48}Ti)	(^{50}Ti,^{52}Ti)	(^{50}Ti,^{52}V)	(^{50}Ti,^{52}Cr)	(^{50}Ti,^{53}V)	(^{50}Ti,^{53}Cr)	(^{50}Ti,^{54}Cr)
Q^a_{gg} (MeV)	−3.4	−2.6	+0.7	+3.1	+2.0	+3.1	+6.0
Q^b_{opt} (MeV)	0	0	+2.1	+4.0	+2.1	+4.0	+4.0
Q^c_{mp} (MeV)	−5	−4	−9	−5	−7	−9	−8

[a] Q_{gg} = g.s.-g.s. Q value.
[b] Q_{opt} = optimum transfer Q value. Values are obtained using Eq. 3.5.7 of Ref. 13, with $r_i = r_f = 12.6$ fm.
[c] Q_{mp} = most probable Q value.

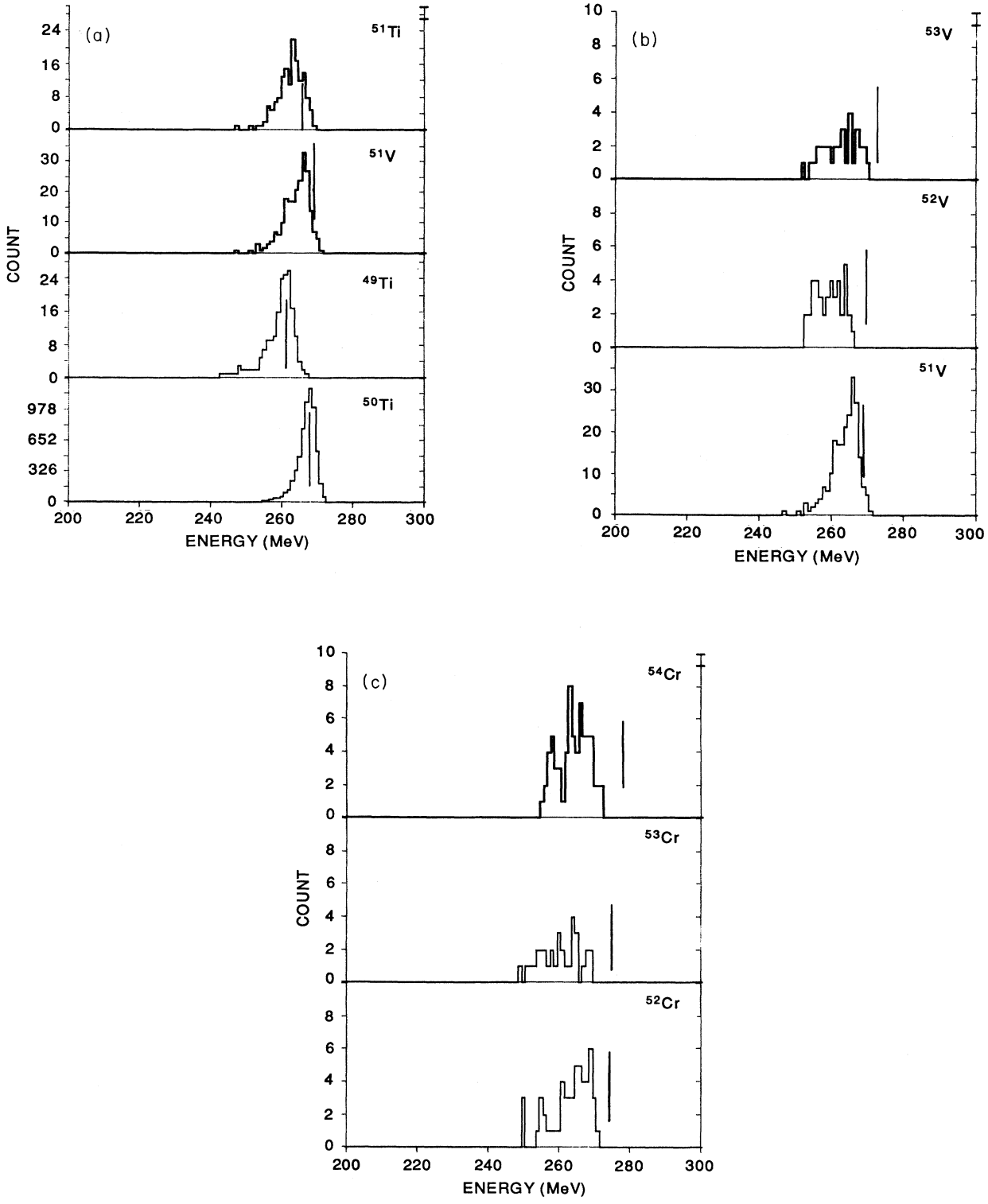

FIG. 5. (a) Energy spectra of reaction products from the incident and single-nucleon-transfer reactions at $E=107.3$ MeV and $\theta_l=14°$. The vertical lines show the positions of Q_{gg}. (b) Energy spectra of vanadium isotopes at $E=107.3$ MeV and $\theta_l=14°$. The vertical lines show the positions of Q_{gg}. (c) Energy spectra of chromium isotopes at $E=107.3$ MeV and $\theta_l=14°$. The vertical lines show the positions of Q_{gg}.

section values for these relative results can be obtained using the normalization factors given in Table II.

F. Transfer probability

Since our interest lies in the sub-barrier region, where interactions take place at relatively large internuclear separation distances, probabilities and apsidal distances are more appropriate quantities for ensuing discussions than are differential cross sections, energies, and angles. The differential cross section for transfer channel i at a particular energy E and angle θ, $(d\sigma/d\sigma\Omega_i)(E,\theta)$, can be transformed to the corresponding transfer probability $P\ [D(E,\theta)]=(d\sigma/d\sigma_{qe})(E,\theta)$, where $(d\sigma/d\Omega_{qe})(E,\theta)=\sum_i(d\sigma/d\Omega_i)(E,\theta)$ is the quasielastic cross section and $D(E,\theta)$ is the apsidal distance of the incident channel, or the distance separating the incident nuclei at the turning point of the classical orbit. $P(D)$ simply gives the probability for the unabsorbed portion of the incident flux going into the exit channel at apsidal distance D. Our previous report[10] contains a more detailed discussion of $P(D)$ and how D is calculated in the presence of nuclear forces.

Transfer probabilities for the $^{50}Ti\rightarrow{}^{51}V$ and $^{50}Ti\rightarrow{}^{49}Ti$ single-nucleon-transfer reactions are shown vs D in Fig. 9. The straight lines that accompany the experimental results give the theoretical trends as predicted by the tunneling theory (see Ref. 10). Overall, experimental results do increase exponentially with decreasing D in a manner characteristic of the tunneling process. Because of the preponderance of elastic yields, deducing reliable results for neutron-transfer channels is difficult. Thus, the $^{50}Ti\rightarrow{}^{49}Ti$ results shown in this figure are rather limited and only an estimate of $P\sim2.5\%$ for $D<12.2$ fm was obtained for the $^{50}Ti\rightarrow{}^{51}Ti$ channel.

P vs D plot for the $^{50}Ti\rightarrow{}^{54}Cr$ channel is shown in Fig. 10. The yield of ^{54}Cr was not observed at $D=12.8$ fm and larger. Yields were too weak for reliable values of P for the $^{50}Ti\rightarrow{}^{52,53}V$ and $^{52,53}Cr$ transitions separately, but reliable values for combined channels could be determined readily. P vs D plots of the $^{52+53}V$ and $^{52+53}Cr$ combined channels are shown in Fig. 11. Except for the smaller magnitude, these results are similar to the ^{54}Cr results shown in Fig. 10.

Although the intensities of the $^{50}Ti\rightarrow{}^{48}Ti$ and $^{50}Ti\rightarrow{}^{52}Ti$, $2n$-transfer channels are not too different from the intensities of other multinucleon-transfer channels, due to the presence of impurities and the preponderance of elastic yield, only rough estimates can be made: $P\sim1\%$ for $D<12.1$ fm for these $2n$-transfer channels.

Notice how large the probabilities for the multinucleon-transfer channels (Figs. 10 and 11) are, rela-

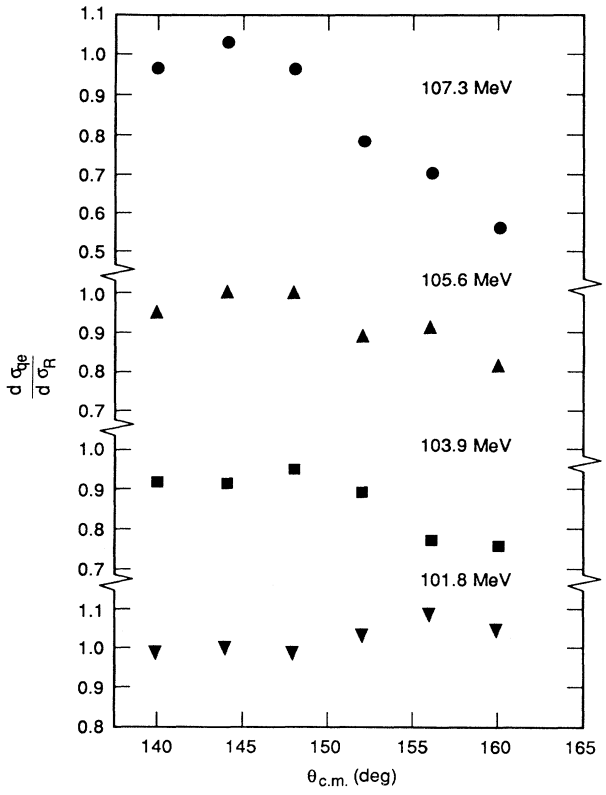

FIG. 6. Angular distributions of the ratio of quasielastic to Rutherford cross section. Statistical errors are smaller than the symbols. The cross-section ratios are subject to up to ±10% systematic error (mainly due to normalization uncertainties).

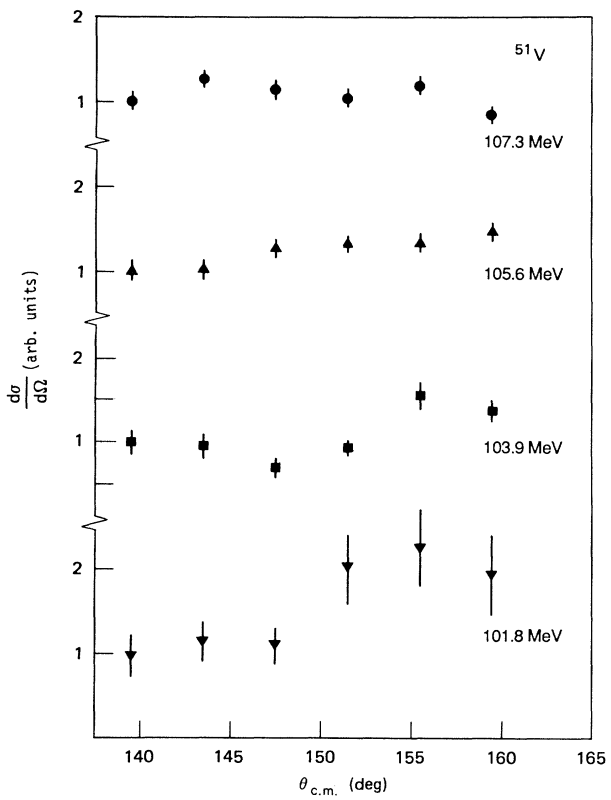

FIG. 7. Angular distributions of ^{51}V from the $^{50}Ti\rightarrow{}^{51}V$, $1p$-transfer reaction. Error bars show statistical errors only. See Table II for the factors needed for absolute cross sections. Systematic error is insignificant.

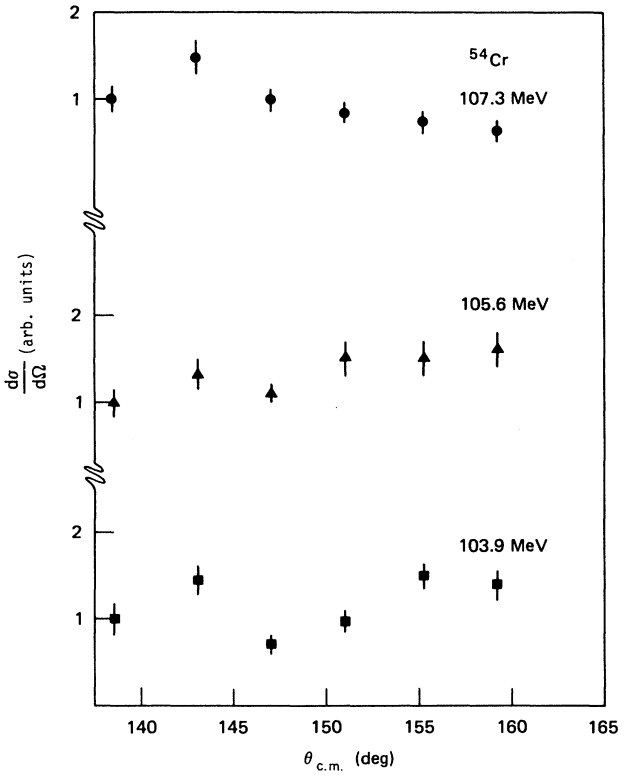

FIG. 8. Angular distributions of ^{54}Cr from the ^{50}Ti→^{54}Cr transfer reaction. Errors shown are statistical errors only. See Table II for the factors needed for absolute cross sections. Systematic error is insignificant.

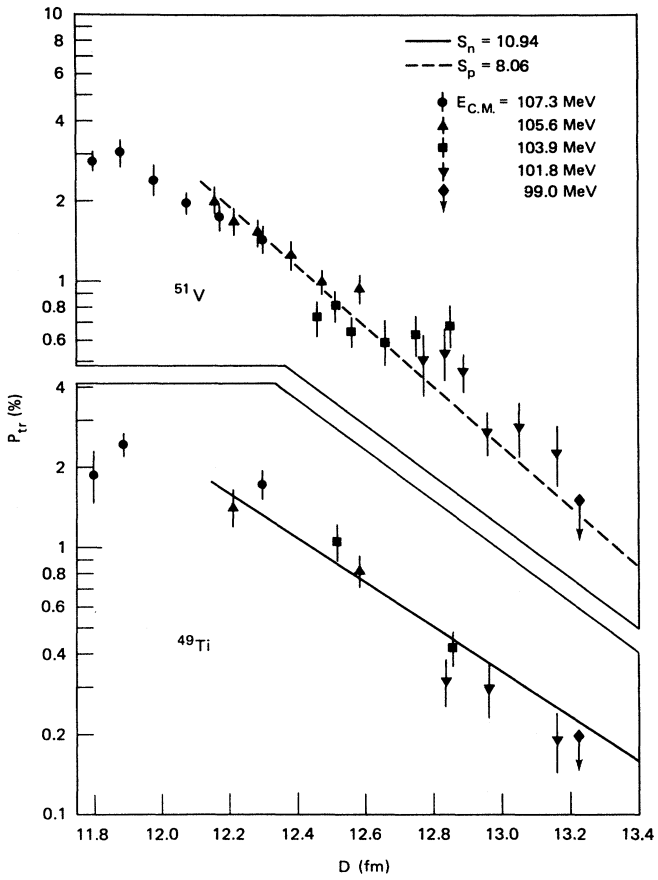

FIG. 9. Transfer probability versus apsidal distance for the ^{50}Ti→^{49}Ti and →^{51}V reactions. Errors shown are statistical errors only. See text for detail. Upper limits only are shown for the lowest energy (99.0 MeV).

tive to the single-nucleon-transfer probabilities (Fig. 9). For example, the probability for transferring four nucleons is nearly half as large as the probability for transferring a single neutron or proton in the 11.8–12.6 fm range.

III. DISCUSSION

The most salient feature observed in this experiment is the appearance of a multitude of reaction products from a variety of multinucleon-transfer reactions at about $D=12.7$ fm. Probabilities relative to single-nucleon-transfer channels are simply too large for the multinucleon-transfer products if they are to result from

TABLE II. Factors for converting results of Figs. 7 and 8 to cross sections in mb/sr. Values of conversion factors are subject to up to ±10% systematic error (mainly due to normalization uncertainties).

$E_{c.m.}$ (MeV)	(^{50}Ti,^{51}V)	(^{50}Ti,^{54}Cr)
101.8	0.71	
103.9	0.86	0.45
105.6	1.17	0.52
107.3	1.08	0.53

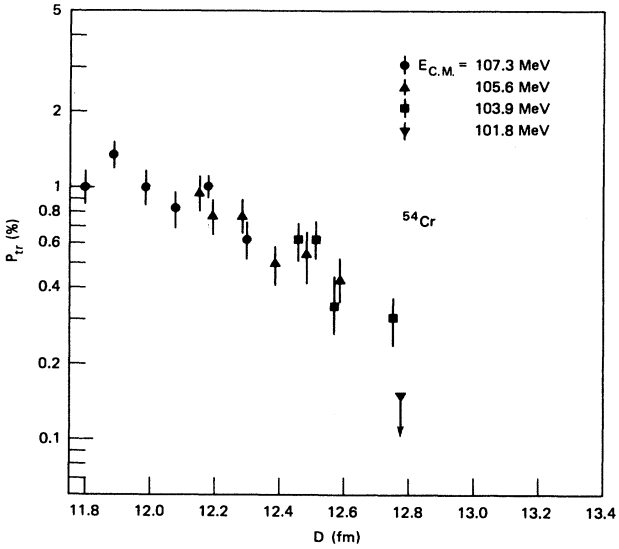

FIG. 10. Transfer probabilities for the ^{50}Ti→^{54}Cr reaction. Errors shown are statistical errors only. Upper limit only is shown for the lowest energy (101.8 MeV).

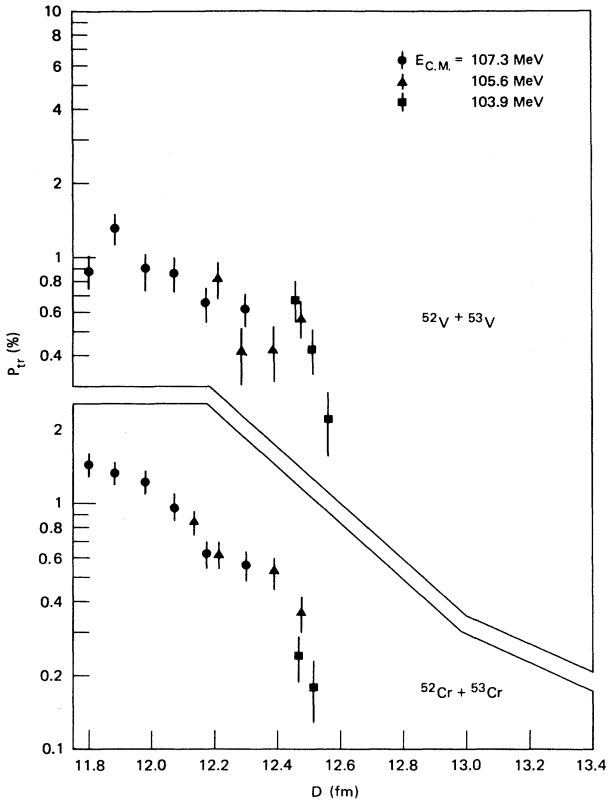

FIG. 11. Transfer probabilities for the $^{50}Ti \rightarrow ^{52+53}V$ and $\rightarrow ^{52+53}Cr$ reactions. Statistical errors only are shown.

a well-established, low-energy transfer mechanism, namely successive nucleon tunneling: based on measured $1p$- and $1n$-transfer probabilities, the probability for transferring three or more nucleons is less 0.03% in the entire D range. One might argue that, if, for example, populated by cluster tunneling (rather than by successive tunnelling), the probability for a particular channel can be as large as the observed values, since such an alternative transfer process is not related to single-nucleon-transfer processes. Even so, it is highly unlikely that all seven observed multinucleon-transfer channels happened to be populated by such mechanisms. Nor is it likely that the magnitude of resulting probabilities for seven different channels would be similar, even if the alternative mechanisms did prevail. Furthermore, as shown in Table I, the average Q values are much too negative relative to the corresponding optimum transfer Q values for the multinucleon-transfer products to result from the conventional mechanism. A thorough discussion of Q value dependence of P can be found in Ref. 12.

The binary nature and the variety of exit channels populated and the damping in the kinetic energies are very reminiscent of characteristics one associates with the more familiar deep-inelastic reactions (see Ref. 13, for example). In a typical deep-inelastic reaction, the formation of a quasimoleculelike configuration follows the initial hard contact between the incident nuclei; and it is the subsequent decay of this configuration (which favors channels where some nucleon, energy, and angular momentum were transferred) that populates binary exit channels. The kinetic energy is damped by the friction that accompanies the nucleon transfer while in the quasimolecular configuration (see Swiatecki,[14] for example).

Based on these close parallels between the present and the deep-inelastic reactions just noted, it is very tempting to associate the onset of the multinucleon-transfer reactions with the beginning, or early phase, of deep-inelastic reactions. And the observation of deep-inelastic events at sub-barrier energies for the Ni+Sn systems[5] supports this association. There are, however, outstanding differences in circumstances of these reactions which counter or weaken this association. Foremost among these circumstances are the energy regime and the angular range. Deep-inelastic reactions typically occur at above barrier energies, but the present reactions were observed at sub-barrier energies; products from deep-inelastic reactions are confined to a narrow angular range near the grazing angle, but the present observations were restricted to large back angles. The difference in energy regimes implies a hard contact and a relatively small internuclear separation for deep-inelastic reactions versus a softer touch and larger separations for the sub-barrier results; the difference in angular range pertains to peripheral versus more central collision.

A simple mechanism that gives a qualitative account of this as well as the fusion[8] experiment can be found in low-energy neck formation theories,[2,15] when they are extended to include binary decays. In these theories, a neck forms during a head-on collision between heavy ions at sub-barrier energies as the collision partners approach the turning point, where they are separated by a certain critical distance. But the neck configuration eventually leads to either coalescence or reseparation, since it is not stable. Coalescence enhances fusion; reseparation boosts binary reactions.

A vital link connecting the above-described neck formation to quasielastic reactions was first suggested in Ref. 3 by Stelson. In Refs. 3 and 8, fusion cross-section data for projectiles ranging from ^{16}O to ^{64}Ni were analyzed with the distributed-barrier model, where the fusion barrier is a distributed quantity with a well-defined threshold and mean. It was found that the threshold energy required is closely correlated with the separation energy of the least bound neutron of the projectile or target. Based on this finding, he suggested that neutron-transfer reactions precipitate the neck formation in the following manner. The mechanism for transferring the least-bound neutron switches from tunneling to free flow beginning at the internuclear separation distance where the tunneling probability first becomes 100% and thus saturates. The saturation occurs once the overlap of the neutron shell-model potentials for target and projectile becomes sufficient that the barrier between them is lower than the energy of the least-bound neutron, thus permitting free flow of the neutron, at the threshold energy.

The fusion threshold determined from measured cross sections (shown in Fig. 1) for the present system is 102.4 MeV and the corresponding distance where the neutron free flow can begin is 12.6 fm. As can be seen in Figs. 10

and 11, the onset of multinucleon-transfer reactions also occurs near this distance. The similarity of these distances is consistent with neck formation being the underlying cause of enhancing, or boosting, of both multinucleon-transfer and fusion reactions and supports the suggestion that the neutron-transfer process is the catalytic reaction. In this connection, we note, in passing, that experimental results (fusion cross sections and the sum of transfer probabilities) indicate the neck configuration is as likely to reseparate as to coalesce near the onset, or threshold.

Features seen in the energy spectra of single-nucleon-transfer reactions [see Figs. 4 and 5(a)] further strengthen the neutron-transfer catalysis scenario. The value of D for the results shown in Fig. 4 is 12.9 fm, and one expects "normal" transfer features in these results, since this distance is beyond that where the neck begins to form. Single-nucleon-transfer spectra shown in Fig. 4 are normal in that the average Q values are the same as the optimum transfer Q values (see Table I). On the other hand, $D=12.0$ fm, well inside the critical distance, for the results shown in Fig. 5(a); accordingly, one expects the effects of the neck to be manifested in these results. The peaks seen in Fig. 5(a) are rather skewed relative to those of Fig. 4 and their average Q values are shifted down significantly, indicating the neck contribution goes to excited transitions.

Although a complete understanding of reactions reported here may be as yet unrealized, certain findings uncovered in this study can be exploited advantageously. As an example, consider the shape of ^{54}Cr and ^{89}Y nuclei at the moment of reseparation at some sub-barrier energy. The average kinetic energy of this exit channel is less than that of the incident channel, although the Coulomb repulsion is stronger. In order for this to happen, the internuclear distance at the moment of separation must have been larger than the apsidal distance where the neck first began to form. This increase in distance necessarily implies that one or both of the exciting nuclei are very much elongated along the representation direction (prolate elongation). We have demonstrated that the ^{54}Cr+^{89}Y and other channels can be isolated cleanly, and they have relatively large cross sections (about 1 mb/sr). These channels are quite amenable to fragment–gamma-ray coincidence studies that provide information pertaining to nuclear shape, energy division (between fragments), and fast versus slow elongation.

IV. SUMMARY AND CONCLUSION

A multitude of products from binary exit channels that require transfer of two or more nucleons emerge at large back angles as the collision partners (^{50}Ti and ^{93}Nb) approach each other to a certain, critical apsidal distance. The Q value is broadly distributed, and its average is much less than the corresponding optimum value for all these multinucleon-transfer channels. The value of this distance is about 12.6 fm, more than 1 fm outside the Coulomb barrier. This distance coincides with the closest approach distance in a head-on collision at the experimental fusion threshold, suggesting a common underlying cause for the onset of multinucleon-transfer reactions and the fusion threshold. The energy of reaction products is distributed around the optimum Q value for the single-neutron-transfer channels at larger apsidal distances, but the energy distribution becomes broader at smaller distances owing to additional contributions. Thus, unlike the case[16] where sub-barrier fusion cross sections are enhanced at the expense of transfer reactions, transfer cross sections, as well as fusion cross sections, are enhanced in this experiment.

Qualitatively, the experimental results are entirely consistent with the neck formation theories. But, quantitative comparisons were not attempted since the present state of neck-formation theories is not amenable to such comparisons yet. The changes observed in the Q-value distribution for single-nucleon-transfer channels with apsidal distance support the suggestion made earlier that the neck formation is precipitated by the transfer of the least bound neutron of the system. Here again, quantitative comparisons are very much needed to firm up this interesting and intuitively appealing catalytic mechanism.

It would be very interesting to extend the present study to the deep-inelastic reaction regime. A detailed evolution of Z, M, and Q-value distributions of reaction products toward traditional deep-inelastic regime observed as function of increasing energy and angular momentum from such a study would provide valuable information pertaining to the separate role played by the tangential, or rotational, and radial kinetic energy.

Irrespective of mechanisms involved, multinucleon-transfer reaction products observed in this experiment emerge with prolate elongation. As we have demonstrated cross sections for these products are relatively large and these products can be isolated cleanly, making them quite amenable for fragment–gamma-ray-coincidence measurements from which information pertaining to nuclear shape, energy partition between fragments, etc., can be obtained.

ACKNOWLEDGMENTS

This research was supported by the Division of High Energy and Nuclear Physics, U.S. Department of Energy, under Contract No. DE-AC05-84OR21400 with Martin Marietta Energy Systems, Inc. We acknowledge a NATO grant for partial support.

[1]S. Landowne and S. C. Pieper, Phys. Rev. C **29**, 1352 (1984); R. A. Broglia *et al.*, Phys. Lett. **133B**, 34 (1983).

[2]C. E. Aguiar, V. C. Barbosa, L. F. Canto, and R. Donangello, Nucl. Phys. **A472**, 571 (1987); A. Iwamoto and K. Harada, Z. Phys. A **326**, 201 (1987); J. Schneider and H. H. Wolter, in *Heavy Ion Interactions Around the Coulomb Barrier,* edited by C. Signorini *et al.* (Springer-Verlag, Berlin, 1988), p. 14.

[3]P. H. Stelson, Phys. Lett. B **205**, 190 (1988).

[4]T. Udagawa, B. T. Kim, and T. Tamura, Phys. Rev. C **32**, 123 (1985); T. Udagawa and T. Tamura, *ibid.* **29**, 1922 (1984).
[5]F. L. H. Wolfs, Phys. Rev. C **36**, 1379 (1987).
[6]A. M. Stefanini *et al.*, Phys. Lett. B **185**, 15 (1987).
[7]L. Corradi *et al.*, Z. Phys. (in press).
[8]P. H. Stelson, H. J. Kim, M. Beckerman, D. Shapira, and R. L. Robinson, Phys. Rev. C **41**, 1584 (1990).
[9]W. Dunnweber, H. Morinaga, and D. E. Alburger, Phys. Lett. **106B**, 47 (1981); H. Wegmann, W. Kutschera, and H. Morinaga, *ibid.* **49B**, 437 (1974); G. Wirth *et al.*, in *Heavy Ion Interactions Around Coulomb Barrier,* edited by C. Signorini *et al.* (Springer-Verlag, Berlin, 1988), p. 84.
[10]H. J. Kim, J. Gomez del Campo, M. M. Hindi, D. Shapira, and P. H. Stelson, Phys. Rev. C **38**, 2081 (1988).
[11]R. O. Sayer, Rev. Phys. Applique **12**, 1543 (1977); K. Shima, T. Ishihara, and T. Mikumo, Nucl. Instrum. Methods **200**, 605 (1982).
[12]See, for example, W. von Oertzen *et al.*, Z. Phys. A **191**, 399 (1987).
[13]W. U. Schroder and J. R. Huizenga, in *Treatise on Heavy-Ion Science,* edited by D. A. Bromley (Plenum, New York, 1984), Chap. 3, Vol. 2.
[14]W. J. Swiatecki, Phys. Scr. **24**, 113 (1981); in *Semiclassical Descriptions of Atomic and Nuclear Collisions,* edited by J. Bang and J. de Boer (North-Holland, Amsterdam, 1985), p. 281.
[15]V. S. Ramamurthy, A. K. Mohanty, S. K. Kataria, and G. Rangarajan, Phys. Rev. C **41**, 2702 (1990); C. E. Aguiar *et al.*, *ibid.* **38**, 541 (1988).
[16]R. A. Broglia *et al.*, Phys. Rev. C **27**, 2433 (1983).